20. Pavlov, V. V., Pisarev, R. V., Kirilyuk, A. & Rasing, T. Observation of a transversal nonlinear magneto-optical effect in thin magnetic garnet films. *Phys. Rev. Lett.* **78,** 2004–2007 (1997).
21. Novoselov, K. S., Geim, A. K., van der Berg, D., Dubonos, S. V. & Maan, J. C. Domain wall propagation on nanometer scale: coercivity of a single pinning center. *IEEE Trans. Magn.* **38,** 2583–2585 (2002).
22. Peeters, F. M. & Li, X. Q. Hall magnetometer in the ballistic regime. *Appl. Phys. Lett.* **72,** 572–574 (1998).
23. Kent, A. D., von Molnar, S., Gider, S. & Awschalom, D. D. Properties and measurement of scanning tunneling microscope fabricated ferromagnetic particle arrays. *J. Appl. Phys.* **76,** 6656–6660 (1994).
24. Li, Y. Q. *et al.* Hall magnetometry on a single iron nanoparticle. *Appl. Phys. Lett.* **80,** 4644–4646 (2002).
25. Hengstmann, T. M., Grundler, D., Heyn, C. & Heitmann, D. Stray-field investigation on permalloy nanodisks. *J. Appl. Phys.* **90,** 6542–6544 (2001).
26. Schuh, D., Biberger, J., Bauer, A., Breuer, W. & Weiss, D. Hall-magnetometry on ferromagnetic dots and dot arrays. *IEEE Trans. Magn.* **37,** 2091–2093 (2001).
27. Vergne, R., Cotillard, J. C. & Porteseil, J. L. Some statistical aspects of magnetization processes in ferromagnetic bodies—motion of a single 180-degrees Bloch wall in an imperfect crystalline medium. *Rev. Phys. Appl.* **16,** 449–476 (1981).
28. Wunderlich, J. *et al.* Influence of geometry on domain wall propagation in a mesoscopic wire. *IEEE Trans. Magn.* **37,** 2104–2107 (2001).
29. Kim, D. H., Choe, S. B. & Shin, S. C. Direct observation of Barkhausen avalanche in Co thin films. *Phys. Rev. Lett.* **90,** 087203 (2003).
30. Magnus, K. *Vibrations* (Blackie & Son, London, 1965).
31. Acheson, D. *From Calculus to Chaos* (Oxford Univ. Press, Oxford, 1997).

**Acknowledgements** This research was supported by the EPSRC (UK). We thank S. Gillott and M. Sellers for technical assistance and J. Steeds for advice on dislocation motion. S.V.D. also acknowledges support from Russian Ministry of Science and Technology.

**Competing interests statement** The authors declare that they have no competing financial interests.

**Correspondence** and requests for materials should be addressed to A.K.G. (geim@man.ac.uk).

# Subwavelength-diameter silica wires for low-loss optical wave guiding

**Limin Tong[1,2], Rafael R. Gattass[1], Jonathan B. Ashcom[1]*, Sailing He[2], Jingyi Lou[2], Mengyan Shen[1,3], Iva Maxwell[1] & Eric Mazur[1]**

[1]*Department of Physics and Division of Engineering and Applied Sciences, Harvard University, Cambridge, Massachusetts 02138, USA*
[2]*Centre for Optical and Electromagnetic Research and Department of Physics, Zhejiang University, Hangzhou 310027, China*
[3]*Department of Physics, Graduate School of Science, Tohoku University, Sendai, Miyagi 9808578, Japan*

* Present address: Lincoln Laboratory, Massachusetts Institute of Technology, Lexington, Massachusetts 02420, USA

**Silica waveguides with diameters larger than the wavelength of transmitted light are widely used in optical communications, sensors and other applications[1–3]. Minimizing the width of the waveguides is desirable for photonic device applications, but the fabrication of low-loss optical waveguides with subwavelength diameters remains challenging because of strict requirements on surface roughness and diameter uniformity[4–7]. Here we report the fabrication of subwavelength-diameter silica 'wires' for use as low-loss optical waveguides within the visible to near-infrared spectral range. We use a two-step drawing process to fabricate long free-standing silica wires with diameters down to 50 nm that show surface smoothness at the atomic level together with uniformity of diameter. Light can be launched into these wires by optical evanescent coupling. The wires allow single-mode operation, and have an optical loss of less than 0.1 dB mm$^{-1}$. We believe that these wires provide promising building blocks for future microphotonic devices with subwavelength-width structures.**

The fabrication of thin silica wires was first investigated in the nineteenth century, when the mechanical properties of the wires were studied, but their optical properties and applications remained uninvestigated[8,9]. It was not until a century later that researchers began to investigate the optical applications of silica wires made by drawing high-purity glass fibres from a laser-heated melt[10–14]. With a diameter of more than one micrometre, these silica wires allow multimode waveguiding of visible and infrared light. Submicrometre wires allow single-mode operation, but both theoretical and experimental results show that the laser power required for drawing silica submicrometre- or nanometre-diameter wires (SMNWs) with a uniform diameter is impractically large[14,15]. When drawing wires from a flame-heated melt, turbulence and convection make it difficult to control the temperature gradient in the drawing region, and consequently size uniformity is difficult to maintain when the wire diameter is reduced to less than one micrometre. Silica nanowires with diameters ranging from ten to several hundred nanometres have recently been obtained with other methods[16–18], but the diameter fluctuation and sidewall roughness of those wires makes them unsuitable for low-loss optical wave guiding.

Here we introduce a two-step drawing process for fabricating long uniform silica SMNWs by a flame-heated fibre drawing method. First, we use a flame to draw a silica fibre to a micrometre-diameter wire. Second, to obtain a steady temperature distribution in the drawing region while further reducing the wire diameter, we use a tapered sapphire fibre with a tip diameter of about 80 μm to absorb the thermal energy from the flame (Fig. 1). The sapphire fibre taper, which is fabricated using laser-heating growth method[19], confines the heating to a small volume and helps maintain a steady temperature distribution during the drawing. One end of a micrometre-diameter silica wire is placed horizontally on the sapphire tip, and the flame is adjusted until the temperature of the tip is just above the drawing temperature (about 2,000 K). We then rotate the sapphire tip around its axis of symmetry to wind the silica wire around the tip. The wire coil is moved about 0.5 mm out of the flame to prevent melting and the wire is then drawn perpendicular to the axis of the sapphire tip in the horizontal plane at a speed of 1–10 mm s$^{-1}$ to form a SMNW.

Using this technique, we obtained silica SMNWs with diameters down to 50 nm and lengths up to tens of millimetres. Figure 2a shows a scanning electron microscope (SEM) image of a 4-mm-long wire with a diameter of 260 nm; the wire is roughly coiled up to show its length. The maximum diameter variation $\Delta D$ is about 8 nm over the 4-mm length $L$ of the wire, giving $\Delta D/L = 2 \times 10^{-6}$. The excellent uniformity of wires with diameters ranging from 50 to 1,100 nm can also be seen in Fig. 2b–d. Higher-magnification transmission electron microscope (TEM) images of a 240-nm-

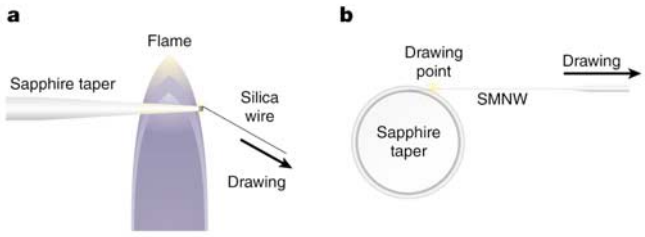


**Figure 1** The second step in the fabrication process of silica submicrometre- and nanometre wires (SMNWs). **a**, Schematic diagram of the drawing of the wire from a coil of micrometre-diameter silica wire wound around the tip of a sapphire taper. The sapphire taper is heated with a $CH_3OH$ torch with a nozzle diameter of about 6 mm. The wire is drawn in a direction perpendicular to the sapphire taper. **b**, Magnified view of the drawing process. The sapphire taper ensures that the temperature distribution in the drawing region remains steady.

diameter wire and of the sidewall of a 330-nm-diameter wire (Fig. 2e and f) show no visible irregularity in the surface of the wires. The typical sidewall root-mean-square roughness of these wires is less than 0.5 nm. The electron microscope pictures in Fig. 2 show that the wires reported here have much better uniformity of diameter and surface smoothness than submicrometre- or nanometre-width wires, strips or other structures obtained by other methods[16–18,20–23].

Because of their length and flexibility, the silica SMNWs can readily be manipulated under an optical microscope. For example, Fig. 3a shows a 520-nm-diameter silica wire that is elastically bent to form a microscopic ring with a diameter of less than 15 μm; Fig. 3b shows two 330-nm-diameter wires that are twisted together. The wires do not break when bent and/or twisted, indicating that they have excellent flexibility and mechanical properties. Using the Young's modulus of silica (73.1 GPa), we find that the tensile strength of the wire in Fig. 3a is at least 2.5 GPa (refs 24, 25). The wires can be bent much more sharply than shown in Fig. 3a. Figure 3c, for example, shows a 280-nm-diameter wire bent to a radius of 2.7 μm, indicating a tensile strength exceeding 4.5 GPa. By bending them to the point of fracture, we find that the tensile strength of the wires is typically higher than 5.5 GPa. Using plastic bending, we have achieved bending radii of less than 1 μm.

We investigated the optical properties of the silica SMNW by sending light into them using evanescent coupling. First, a SMNW is suspended in air, with one end fixed to a support and the other end connected to the fibre taper from which it was drawn (fibre taper 1 in Fig. 4a). Light is then coupled into the SMNW through a second fibre taper. The launching wire from this second taper attaches itself to the guiding wire because of a van der Waals attraction between the two. To reduce the contribution from scattered light, both tapers are gold-coated except for the region used for evanescent coupling. Figure 4b shows an optical micrograph of the coupling between a 390-nm-diameter launching wire and a 450-nm-diameter SMNW; Fig. 4c shows a 360-nm-diameter wire guiding light of 633-nm wavelength from the left. The light is intercepted at the right by a supporting 3-μm wire to show that the amount of light scattered by the wire is small compared to that guided by it. In Fig. 4d, a 550-nm-diameter wire guides 633-nm light in air (on the left) and along the surface of a $MgF_2$ crystal (on the right). Because the refractive index of $MgF_2$ is lower than that of silica (1.39 versus 1.46), the light continues to be guided by the wire on the $MgF_2$ surface, demonstrating the possibility of integrating SMNWs with low-index substrates for device applications. We also determined that a 620-nm-diameter wire immersed in water guides light, demonstrating the possibility of using these wires for chemical and biosensing in liquid media.

We determined the optical loss of the SMNWs by measuring their transmission as a function of the length $L$ between the coupling region and taper 1 (see Fig. 4a). To maintain the same coupling efficiency between the launching and guiding wires, we adjust the overlap of the two wires until the output from fibre taper 1 is maximized. Figure 4e shows the optical loss at wavelengths of 633 and 1,550 nm for various SMNW diameters. At 633 nm, the optical

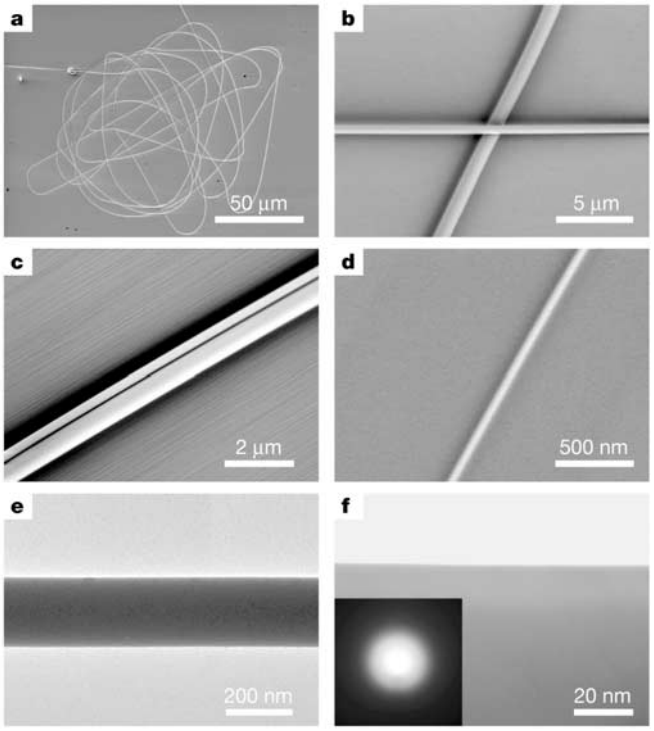


**Figure 2** Electron micrographs of SMNWs. **a**–**d**, SEM images; **e**,**f**, TEM images. **a**, A coiled 260-nm-diameter silica wire with a total length of about 4 mm. **b**, Two crossed 570-nm and 1,100-nm diameter wires. **c**, Two parallel 170-nm and 400-nm diameter wires. **d**, A silica nanowire with a diameter of about 50 nm. **e**, A 240-nm-diameter silica wire. **f**, The surface of a 330-nm-diameter silica wire; the electron diffraction pattern (inset) demonstrates that the wire is amorphous.

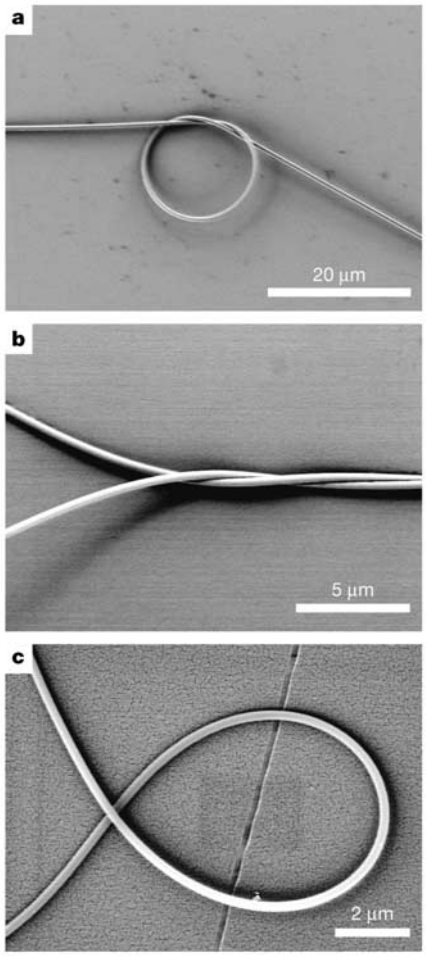


**Figure 3** Micromanipulation and flexibility of SMNWs. **a**, SEM image of a 15-μm-diameter micro-ring made with a 520-nm-diameter silica wire. **b**, SEM image of two twisted 330-nm-diameter wires. **c**, SEM image of a bent 280-nm-diameter silica wire with a bending radius of 2.7 μm.

loss of a 190-nm-diameter wire is about 1.7 dB mm$^{-1}$, which is much lower than the optical loss of other subwavelength-structures such as metallic plasmon waveguides[26–28].

The increasing loss with decreasing wire diameter can be attributed to surface contamination: as the wire diameter is reduced below the wavelength, more light is guided outside the wire as an evanescent wave and becomes susceptible to scattering by surface contamination. Calculations show that the critical diameter for single-mode operation of a silica wire is about 450 nm at 633-nm wavelength and 1,100 nm at 1,550-nm wavelength[29], and that about 20% of the energy propagates outside the silica core under those conditions. Figure 4e shows that wires with these diameters have an optical loss below 0.1 dB mm$^{-1}$. For smaller diameters, more light propagates outside the silica core as an evanescent wave. Evanescent wave propagation is extremely useful for enhancing the performance of devices such as optical sensors.

Because of the large index contrast between silica and air, silica SMNWs can be bent sharply without incurring large bending losses. Using a three-dimensional finite-difference time domain simulation[30], we find a bending loss of less than 0.3 dB for a 90° turn with a bending radius of 5 μm in an air-clad 450-nm-diameter silica wire (for light of 633-nm wavelength). These results indicate that the silica SMNWs are also suitable for applications where tight waveguide bends are desired. Using two probes from a scanning tunnelling microscope for micromanipulation, we were able to successfully guide 633-nm wavelength light through a bend with a 5.6-μm radius in a silica wire with a diameter of about 510 nm (see Fig. 4f). As can be seen in the figure, the intensity of scattered light after the bend is not greatly reduced, indicating that the bending loss is low. The ability to guide light through sharp bends is especially useful for miniaturization of photonic devices. Also, with low bending loss, micro-rings made from these wires (such as the one shown in Fig. 3a) can be incorporated into photonic devices such as optical microresonators for optical communication or optical sensing. For example, we used a 950-nm-diameter SMNW to make a ring with a 75-μm radius similar to the one shown in Fig. 3a; preliminary measurements show that the ring has $Q$ factor of about 1,500 at a wavelength of 1,550 nm.

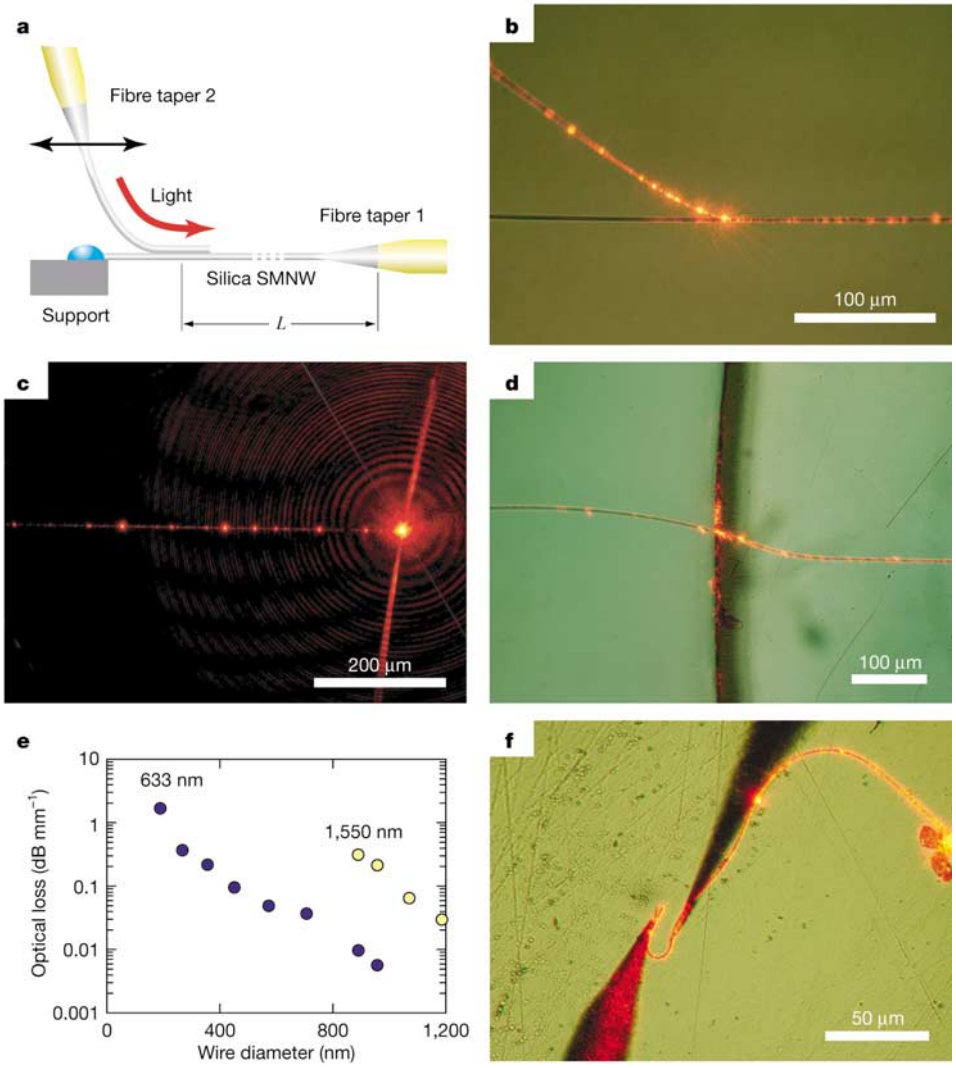


**Figure 4** Optical characterization of SMNWs. **a**, Schematic diagram for launching light into a silica wire using evanescent coupling. **b**, Optical microscope image of a 390-nm-diameter taper coupling light into a 450-nm-diameter silica wire. **c**, Long-time exposure micrograph of 633-nm wavelength light guided by a 360-nm-diameter silica wire in air, and intercepted by a 3-μm guiding wire on the right. **d**, Optical microscope image of 633-nm-wavelength light guided by a 550-nm-diameter silica wire with its left half suspended in air and its right half placed on a $MgF_2$ crystal. **e**, Measured optical loss of silica wires at 633 nm (filled blue circles) and 1,550 nm (filled yellow circles). **f**, Optical microscope image of 633-nm light travelling through a sharp bend with a radius of 5.6 μm in a 510-nm-wide silica wire.

The wires reported here are suitable for low-loss optical wave guiding, and will be promising components in future microphotonic devices for various applications, such as optical communications and optical sensing. Owing to their excellent uniformity, large length, high flexibility, and strength, these wires can be manipulated and assembled with high accuracy and used as micro- or nanoscale tools in physical, chemical, biological, microelectronic and materials research. □

Received 22 August; accepted 4 November 2003; doi:10.1038/nature02193.


1. Yamane, M. & Asahara, Y. *Glasses for Photonics* (Cambridge Univ. Press, Cambridge, UK, 2000).
2. Murata, H. *Handbook of Optical Fibers and Cables* 2nd edn (Marcel Dekker, New York, 1996).
3. Mynbaev, D. K. & Scheiner, L. L. *Fiber-Optic Communications Technology* (Prentice Hall, New York, 2001).
4. Marcuse, D. Mode conversion caused by surface imperfections of a dielectric slab waveguide. *Bell Syst. Tech. J.* **48,** 3187–3215 (1969).
5. Marcuse, D. & Derosier, R. M. Mode conversion caused by diameter changes of a round dielectric waveguide. *Bell Syst. Tech. J.* **48,** 3217–3232 (1969).
6. Ladouceur, F. Roughness, inhomogeneity, and integrated optics. *J. Lightwave Technol.* **15,** 1020–1025 (1997).
7. Lee, K. K. *et al.* Effect of size and roughness on light transmission in a $Si/SiO_2$ waveguide: experiments and model. *Appl. Phys. Lett.* **77,** 1617–1619 (2000). Erratum. *Appl. Phys. Lett.* **77,** 2258 (2000).
8. Boys, C. V. On the production, properties, and some suggested uses of the finest threads. *Phil. Mag.* **23,** 489–499 (1887).
9. Threlfall, R. *On Laboratory Arts* (Macmillan, London, 1898).
10. Knight, J. C., Cheung, G., Jacques, F. & Birks, T. A. Phase-matched excitation of whispering-gallery-mode resonances by a fiber taper. *Opt. Lett.* **22,** 1129–1131 (1997).
11. Birks, T. A., Wadsworth, W. J. & Russell, P. St. J. Supercontinuum generation in tapered fibers. *Opt. Lett.* **25,** 1415–1417 (2000).
12. Cai, M. & Vahala, K. Highly efficient hybrid fiber taper coupled microsphere laser. *Opt. Lett.* **26,** 884–886 (2001).
13. Kakarantzas, G., Dimmick, T. E., Birks, T. A., Le Roux, R. & Russell, P. St. J. Miniature all-fiber devices based on $CO_2$ laser microstructuring of tapered fibers. *Opt. Lett.* **26,** 1137–1139 (2001).
14. Dimmick, T. E., Kakarantzas, G., Birks, T. A. & Russell, P. St. J. Carbon dioxide laser fabrication of fused-fiber couplers and tapers. *Appl. Opt.* **38,** 6845–6848 (1999).
15. Grellier, A. J. C., Zayer, N. K. & Pannell, C. N. Heat transfer modeling in $CO_2$ laser processing of optical fibres. *Opt. Commun.* **152,** 324–328 (1998).
16. Wang, Z. L., Gao, R. P. P., Gole, J. L. & Stout, J. D. Silica nanotubes and nanofiber arrays. *Adv. Mater.* **12,** 1938–1940 (2000).
17. Pan, Z. W., Dai, Z. R., Ma, C. & Wang, Z. L. Molten gallium as a catalyst for the large-scale growth of highly aligned silica nanowires. *J. Am. Chem. Soc.* **124,** 1817–1822 (2002).
18. Hu, J. Q., Meng, X. M., Jiang, Y., Lee, C. S. & Lee, S. T. Fabrication of germanium-filled silica nanotubes and aligned silica nanofibers. *Adv. Mater.* **15,** 70–73 (2003).
19. Labelle, H. E. & Mlavsky, A. I. Growth of sapphire filaments from melt. *Nature* **216,** 574–575 (1967).
20. Morales, A. M. & Lieber, C. M. A laser ablation method for the synthesis of crystalline semiconductor nanowires. *Science* **279,** 208–211 (1998).
21. Xia, Y., Rogers, J. A., Paul, K. E. & Whitesides, G. M. Unconventional methods for fabricating and patterning nanostructures. *Chem. Rev.* **99,** 1823–1848 (1999).
22. Ito, T. & Okazaki, S. Pushing the limits of lithography. *Nature* **406,** 1027–1031 (2000).
23. Lee, K. K., Lim, D. R., Kimerling, L. C., Shin, J. & Cerrina, F. Fabrication of ultralow-loss $Si/SiO_2$ waveguides by roughness reduction. *Opt. Lett.* **26,** 1888–1890 (2001).
24. Matthewson, M. J., Kurkjian, C. R. & Gulati, S. T. Strength measurement of optical fibers by bending. *J. Am. Ceram. Soc.* **69,** 815–821 (1986).
25. Krause, J. T., Testardi, L. R. & Thurston, R. N. Deviations from linearity in the dependence of elongation upon force for fibers of simple glass formers and of glass optical light guides. *Phys. Chem. Glasses* **20,** 135–139 (1979).
26. Takahara, J., Yamagishi, S., Taki, H., Morimoto, A. & Kobayashi, T. Guiding of a one-dimensional optical beam with nanometer diameter. *Opt. Lett.* **22,** 475–477 (1997).
27. Maier, S. A., Kik, P. G. & Atwater, H. A. Observation of coupled plasmon-polarization modes in Au nanoparticle chain waveguides of different lengths: Estimation of waveguide loss. *Appl. Phys. Lett.* **81,** 1714–1716 (2002).
28. Maier, S. A. *et al.* Local detection of electromagnetic energy transport below the diffraction limit in metal nanoparticle plasmon waveguides. *Nature Mater.* **2,** 229–232 (2003).
29. Snyder, A. W. & Love, J. D. *Optical Waveguide Theory* (Chapman and Hall, New York, 1983).
30. Taflove, A. *Computational Electrodynamics: The Finite-difference Time-domain Method* (Artech House, Boston, 1995).


**Acknowledgements** We thank Y. Lu, Z. Han and B. Tull for assistance in SEM and TEM imaging, and L. Liu and X. Chen for help with numerical simulations. This work was supported by the US National Science Foundation and by the National Natural Science Foundation in China. T.L. acknowledges support from the Centre for Imaging and Mesoscale Structures at Harvard University.

**Competing interests statement** The authors declare that they have no competing financial interests.

**Correspondence** and requests for materials should be addressed to E.M. (mazur@deas.harvard.edu).

# Synthesis of a Möbius aromatic hydrocarbon

**D. Ajami[1], O. Oeckler[2], A. Simon[2] & R. Herges[1]**

[1]*Institut für Organische Chemie, Universität Kiel, Otto-Hahn-Platz 4, 24098 Kiel, Germany*
[2]*Max-Planck-Institut für Festkörperforschung, Heisenbergstraße 1, D-70569 Stuttgart, Germany*

**The defining feature of aromatic hydrocarbon compounds is a cyclic molecular structure stabilized by the delocalization of π electrons that, according to the Hückel rule, need to total $4n + 2$ ($n = 1,2,\ldots$); cyclic compounds with $4n$ π electrons are antiaromatic and unstable. But in 1964, Heilbronner predicted[1] on purely theoretical grounds that cyclic molecules with the topology of a Möbius band—a ring constructed by joining the ends of a rectangular strip after having given one end half a twist—should be aromatic if they contain $4n$, rather than $4n + 2$, π electrons. The prediction stimulated attempts to synthesize Möbius aromatic hydrocarbons, but twisted cyclic molecules are destabilized by large ring strains, with the twist also suppressing overlap of the *p* orbitals involved in electron delocalization and stabilization. In larger cyclic molecules, ring strain is less pronounced but the structures are very flexible and flip back to the less-strained Hückel topology[2,3]. Although transition-state species[4], an unstable intermediate[5] and a non-conjugated cyclic molecule[6], all with a Möbius topology, have been documented, a stable aromatic Möbius system has not yet been realized. Here we report that combining a 'normal' aromatic structure (with *p* orbitals orthogonal to the ring plane) and a 'belt-like' aromatic structure (with *p* orbitals within the ring plane) yields a Möbius compound stabilized by its extended π system.**

Numerous theoretical calculations have been performed to predict the properties of potential Möbius aromatic systems[7–12]. The twist in the π system is usually introduced by a suitable arrangement of *E* and *Z* double bonds. *Trans*-benzene[13] is the smallest conceivable antiaromatic Möbius annulene. It is only a very shallow minimum on the energy hypersurface, with an energy as much as 107 kcal mol$^{-1}$ above benzene[14]. The next-higher Möbius homologue, *trans*-cyclooctatetraene, indeed comes energetically closer to its Hückel (all-*cis* and global minimum) isomer[14]. Nevertheless, with a relative energy of 21.3 kcal mol$^{-1}$, it is expected to be extremely difficult to synthesize. Moreover, there is almost no conjugation between the *E* and the neighbouring *Z* double bonds

Table 1 **Relative stabilities**

| [16]annulene | | | Möbius stabilized [16]annulene | | |
|---|---|---|---|---|---|
| $E_{ref}$ | Topology | Sym. | $E_{ref}$ | Topology | Sym. |
| 0.0 | Hückel | $S_4$ | 0.0 | Möbius | $C_1$ |
| 2.0 | Hückel | $C_1$ | 0.3 | Möbius | $C_2$ |
| 5.1 | Möbius | $C_1$ | 2.8 | Möbius | $C_2$ |
| 7.6 | Möbius | $C_2$ | 2.8 | Möbius | $C_1$ |
| 15.8 | Möbius | $C_2$ | 6.7 | Möbius | $C_1$ |
| 51.4 | Möbius | $C_2$ | 7.0 | Hückel | $C_s$ |
| | | | 8.3 | Möbius | $C_1$ |

Calculated relative stabilities ($E_{ref}$ in kcal mol$^{-1}$) of the most stable isomers of the parent [16]annulene and of our modified [16]annulene at the B3LYP/6-31G* level of DFT.